IEEE Photonics Journal
An IEEE Photonics Society Publication

Open Access

Generation of Terahertz Vortices Using Metasurface With Circular Slits

Volume 6, Number 6, December 2014

Hailong Zhou
Jianji Dong
Siqi Yan
Yifeng Zhou
Xinliang Zhang

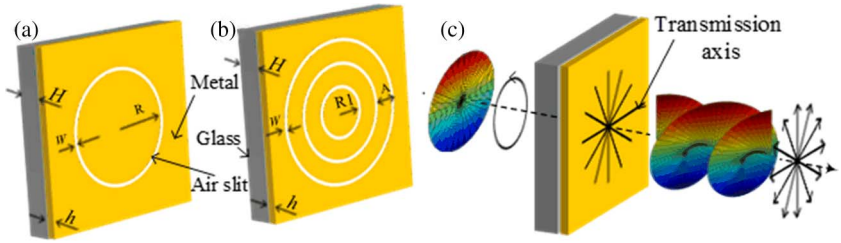

DOI: 10.1109/JPHOT.2014.2363424
1943-0655 © 2014 IEEE

IEEE photonics SOCIETY

IEEE

Generation of Terahertz Vortices Using Metasurface With Circular Slits

Hailong Zhou, Jianji Dong, Siqi Yan, Yifeng Zhou, and Xinliang Zhang

Wuhan National Laboratory for Optoelectronics, School of Optoelectronic Science and Engineering, Huazhong University of Science and Technology, Wuhan 430074, China

DOI: 10.1109/JPHOT.2014.2363424

Manuscript received August 19, 2014; revised September 29, 2014; accepted October 2, 2014. Date of publication October 16, 2014; date of current version November 4, 2014. This work was supported in part by the Program for New Century Excellent Talents of the Ministry of Education of China under Grant NCET-11-0168, by the Foundation for the Author of National Excellent Doctoral Dissertation of China under Grant 201139, by the National Natural Science Foundation of China under Grant 11174096, and by the Fundamental Research Funds for the Central Universities, Huazhong University of Science and Technology, under Grant 2014YQ015. Corresponding author: J. Dong (e-mail: jjdong@mail.hust.edu.cn).

Abstract: We propose a metal device containing circular slits to generate a terahertz (THz) orbital angular momentum beam with numerical simulations. The estimation of the polarization extinction ratio is above 20 dB over the bandwidth ranging from 0.3 to 3 THz, and a mode purity of TC $= 1$ or -1 is close to 1 over a wide bandwidth range, except for the area near the deteriorated valley. We analyze the OAM spectrum and find that the main noise comes from an OAM mode of TC $= -3$ or 3. When multiple concentric circular slits are employed, a larger transmittance is obtained without the sacrifice of mode purity. The design of such a device is simple with a size of micrometer order, revealing an option to generate a broadband THz vortex beam.

Index Terms: Orbital angular momentum, terahertz.

1. Introduction

Light beams carrying orbital angular momentum (OAM) are associated with an azimuthal phase structure $\exp(il\theta)$, where θ is the angular coordinate and l is the azimuthal index, defining the topological charge (TC) of the OAM beams [1]. These beams have an OAM of $l\hbar$ per photon ($\hbar$ is Planck's constant h divided by 2π). As a novel radiation, terahertz (THz) radiation has been receiving increasing levels of interest in diverse areas such as communications and the imaging and sensing fields [2]. Therefore, THz devices need to be developed. There are many works about THz wave plates, polarizers, filters, absorbers, etc. [2]–[8]. However, only few works about the THz vortex beam have been reported [9], [10]. In 2013, Zhang *et al.* used the complementary V-shaped antenna structure to generate a THz vortex beam, which requires precise control of the geometric parameters and azimuth of the V-shaped antenna structure. In 2014, the spiral phase plates (SPPs) were designed and fabricated to generate OAM modes at 0.1 THz, but the SPPs are hard to integrate because of their large size and discontinuities that make it difficult to generate a high pure THz OAM beam. In addition, these two approaches are both limited by the single operating wavelength.

In the optical band, it has been reported that OAM beam generation is possible by controlling the localized polarization, such as using an axially symmetric polarizer (ASP) [11]–[13] and

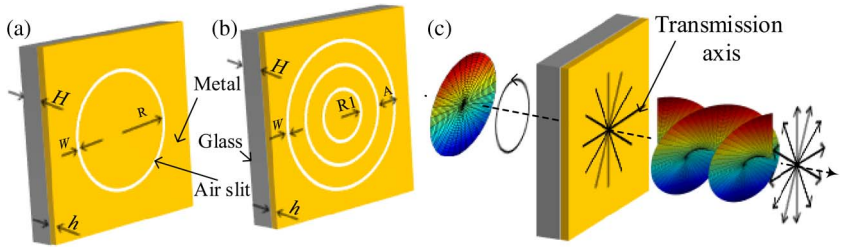

Fig. 1. Schematic structure of the proposed device generating OAM-carrying THz beams. (a) Single slit. (b) Multiple slits. (c) Generating OAM-carrying vector beam.

subwavelength apertures on the metasurface [14], [15]. It is hard to generate high pure OAM beams with those methods because of the discrete geometries of structure. However, the function of localized polarization is still effective and the OAM beams with a high purity can be generated by changing the subwavelength apertures from radial distribution [14], [15] to continuous azimuthal distribution, which is similar to the structure in [16]–[19]. By extending the principle to the THz wave band, the function of localized polarization is still effective and the THz OAM beams with a high purity can be generated.

In this paper, we design a metasurface containing circular subwavelength slits to convert the spin angular momentum (SAM) of the incident THz beam to OAM. Our device has a similar function to that of the ASP, which can be regarded as a radial polarizer. The polarization extinction ratio (PER) is above 20 dB over the bandwidth, ranging from 0.3 THz to 3 THz, and the mode purity of TC $= 1$ (-1) is close to 1 over a wide bandwidth range, except for the area near the deteriorated valley. We analyze the OAM spectrum and find the main noise comes from the OAM mode of TC $= -3$ (3). We can reasonably design the structure and parameters to avoid the deteriorated valley at the expected frequencies. Therefore, when multiple slits are employed, it still has a high purity and keeps a larger transmittance. The structure is very simple with a size of micrometer order, which offers an easy approach to broadband generation of the THz vortex beam.

2. Principle and Structure

Fig. 1(a) presents the schematic structure and geometric parameters of the proposed device. We design a circular subwavelength air slit in a metal (silver) film with a thickness of $h = 200$ nm, as shown in Fig. 1(a), and the metal film is deposited on the silica substrate with a thickness of $H = 3$ μm. The inner radius of the slit is R and the width is W. The subwavelength slit can be regarded as a localized linear polarizer (perpendicular to the slit direction, i.e., radial direction) [14], so we can infer that the proposed device can act as an ASP whose transmission axis is radially distributed [11], [12]. The Jones vector of ASP is given by

$$P = \begin{pmatrix} \cos^2\theta & \cos\theta\sin\theta \\ \cos\theta\sin\theta & \sin^2\theta \end{pmatrix} \tag{1}$$

where θ is the azimuth angle in the beam cross section. The SAM is related to the circular polarization basis. When a right or left circularly polarized THz light with Jones vector of $E_{in} = [1\ \sigma i]^T$ ($\sigma = -1$ or 1, $i = \sqrt{-1}$) normally incidents upon the thin film as shown in Fig. 1(c), the output complex amplitude in the near-field zone can be expressed as

$$E_{out} = \exp(i\sigma\theta)\begin{pmatrix} \cos\theta \\ \sin\theta \end{pmatrix}. \tag{2}$$

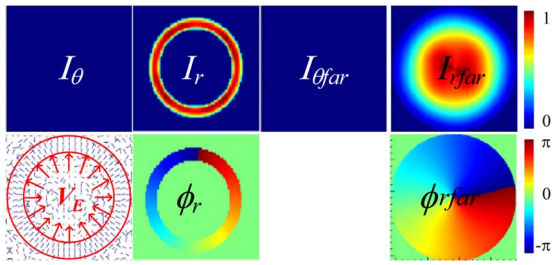

Fig. 2. Spatial distributions of intensity, phase, and electric field vector of generated OAM-carrying vector beams.

The X-component and Y-component of the electric field are defined as E_x and E_y, respectively. We rewrite the output in radial direction and azimuthal direction as

$$E_r = E_x\cos\theta + E_y\sin\theta = \exp(il\theta)$$
$$E_\theta = -E_x\sin\theta + E_y\cos\theta = 0. \tag{3}$$

From Eqs. (2) and (3), it proves this device can convert the SAM of the incident THz beam to OAM (TC $= 1$ or -1) and the vector of electric field is radially polarized as shown in Fig. 1(c). When multiple slits with number of N are employed as shown in Fig. 1(b), whose radii can be expressed as $R_n = R_1 + A(n-1)$ $(n = 1, 2 \ldots N)$, it should have similar functions but keep a larger transmittance. In the simulation, we set the total length and width of the device both as 300 μm. And the source area is 200 μm $\times$ 200 μm so that only the silts can transmit the light. The simulation domain is 500 μm $\times$ 500 μm $\times$ 300 μm.

3. Simulation Results and Analysis

We first set the parameters $W = 6$ μm, $R = 25$ μm, as shown in Fig. 1(a). Assume that a circularly polarized plane wave (taking $E_{in} = [1\ i]^T$ as an example) whose frequency is limited within 0.3–3 THz normally incidents upon the metal film. Fig. 2 presents the intensity patterns, phase patterns and the spatial distribution of the electric field vector at 2.4 THz through three-dimensional finite difference time domain (FDTD) simulations. I_r, ϕ_r, and I_θ are the radial intensity, the radial phase, and the azimuthal intensity in the near-field zone, respectively. I_{rfar}, ϕ_{rfar}, and $I_{\theta far}$ are the radial intensity, the radial phase, and the azimuthal intensity in the far-field zone, respectively. V_E denotes the spatial distribution of the electric field vector, which can be expressed as

$$V_E(\theta) = \frac{\mathrm{Re}[E_{out}\exp(-i\omega t)]}{|\mathrm{Re}[E_{out}\exp(-i\omega t)]|} \tag{4}$$

where ω is the frequency of the incoming wave, t is the time variable, and Re[.] denotes the real part. |.| denotes the modulus of vector.

From Fig. 2, we can see that the simulated results are in good agreement with the theoretical analysis by (2)–(4). In the near-field zone, the azimuthal intensity (I_θ) is close to null compared to the radial intensity (I_r), and the radial phase (ϕ_r) presents a perfect helical phase structure with TC equal to 1. Thus, the output electric field is radially polarized. Moreover, we can analyze the far-field distributions and see that the same characteristics are presented. It is worth noting that the emitted beam in the far-field zone has a non-zero intensity at the beam center (I_{rfar}) which is known as a family of Poincarè or polarization-singular beams [20]–[22]. V_E shows the spatial distribution of the electric field vector. The region between the two red circles covers almost all the energy and the red arrows are the zoom-in indications of the electric field vector in this region. One may notice that these vectors are different from the ones shown in Fig. 1(c). It

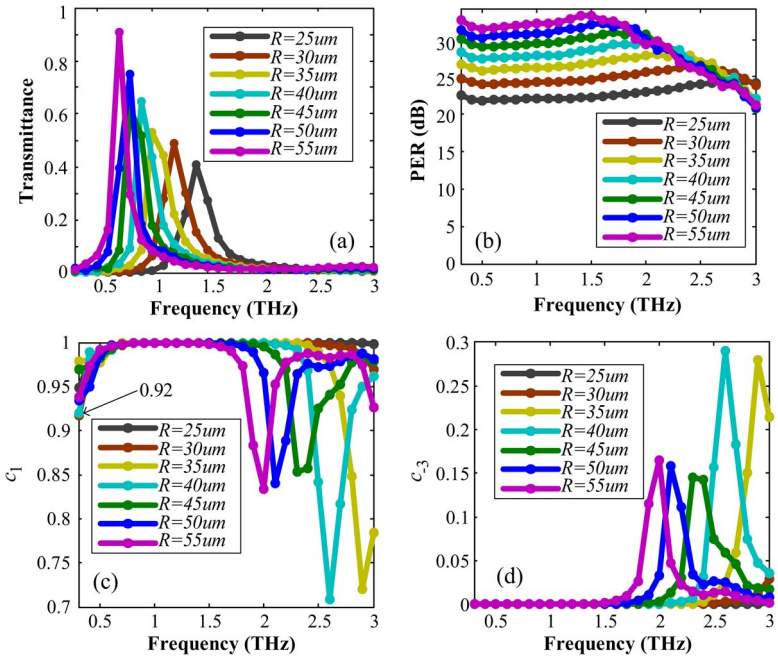

Fig. 3. (a) Transmittance, (b) PER, (c) purity of TC $= 1$, and (d) the main noise of TC $= -3$ under different radius.

is because that we do not consider the helical phase factor of $\exp(i\sigma\theta)$ in Fig. 1(c), and therefore, the electric field vector can be expressed as $[\cos\theta\ \sin\theta]^T$. However, the vectors calculated by FDTD take all factors into account, and therefore, the azimuth of θ and $\theta + \pi$ in Fig. 2 have the same vector, which can be deduced by

$$V_E(\theta + \pi) = V_E(\theta). \tag{5}$$

We then use transmittance, PER, and mode purity to characterize the quality of the generated OAM-carrying vector beams. The PER is defined as $10 \times \log_{10}(P_r/P_\theta)$ where P_r represents the power of radial direction and P_θ represents the power of azimuthal direction. From Eqs. (2) and (3), we can see that the electric field is radially polarized, so we just need calculate the purity of radial direction and this analysis of mode purity is valid only if PER is big enough. The slit is narrow which can be regarded as one-dimensional geometry (azimuthal direction), so we define the mode purity of OAM beam with TC $= l$ as

$$c_l = \frac{\left| \int_0^{2\pi} \frac{1}{2\pi} E_r(\theta) \exp(-il\theta) d\theta \right|^2}{\int_0^{2\pi} \frac{1}{2\pi} |E_r(\theta)|^2 d\theta}. \tag{6}$$

We set $W = 6$ μm and vary R from 25 μm to 55 μm, then calculate the transmittance, PER, and purity $(\text{TC} = 1)$, which are shown in Fig. 3(a)–(c). Fig. 3(a) displays the transmittance when the area of plane source is 200 μm $\times$ 200 μm. One can see that the transmittance is low except in the region near the peaks. The reason is because the effective transmission area (area of slits) is much smaller than the one of the plane source, and the peaks are caused by the existence of transmission resonances [23]. The PER shown in Fig. 3(b) is above 20 dB over the bandwidth ranging from 0.3 THz to 3 THz and the mode purity shown in Fig. 3(c) is close to 1

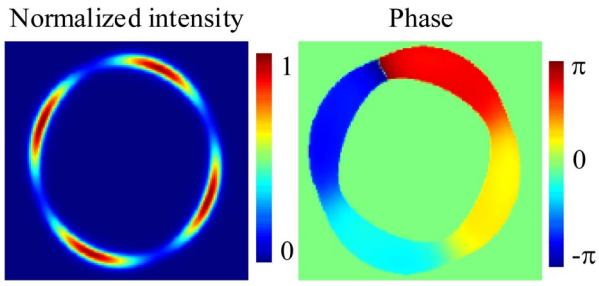

Fig. 4. Intensity and phase distributions of generated OAM-carrying vector beams at 2 THz when R = 55 μm.

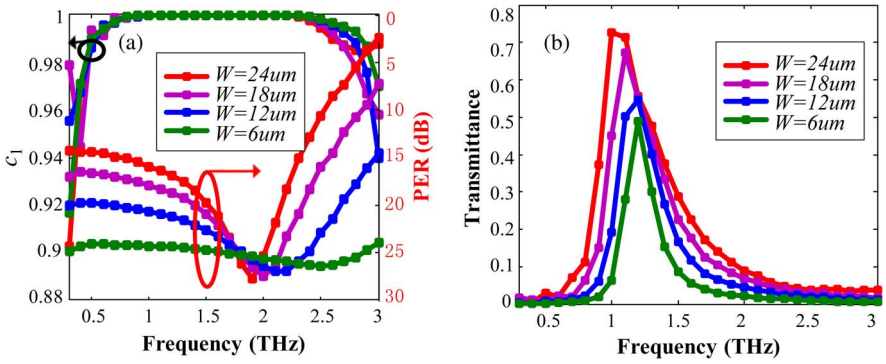

Fig. 5. (a) PER and purity of TC = 1 and (b) transmittance under different width when R = 30 μm.

over the middle area except the area near the deteriorated valley. When the radius is not more than 30 μm, the mode purity can reach 0.92 over the whole bandwidth. For larger radius, a deteriorated valley will appear where the purity becomes poor and the deteriorated frequencies decrease with increasing the radius of the slit. But it still keeps a high purity near both sides of the deteriorated valley. We analyze the OAM spectrum and find the main noise comes from the OAM mode of TC $= -3$. As shown in Fig. 3(d) the share of this mode is complementary to the mode of TC = 1 and the sum of these two modes is close to 1 over all the bandwidth. Taking $R = 55$ μm as an example, Fig. 4 displays the intensity and phase distributions of generated OAM-carrying vector beams at the deteriorated valley of 2 THz. The phase distribution presents a rough helical phase pattern with TC equal to 1 in the near field. The intensity distribution has four peaks, which are caused by the interference of the two OAM modes with TC equal to -3 and 1. We analyze the eigenmodes of the slit waveguide and find the OAM mode of TC $= -3$ is an eigenmode. In addition, we find that the noise of TC $= -3$ will increase when increasing the thickness of the metal film; therefore, the mode crosstalk may be caused by the mode coupling in the metal waveguide at a certain frequency range.

Similarly, when a right circularly polarized light is normally incident on the metal film, it will generate the OAM light with TC equal to -1 and a deteriorated valley of mode purity will appear where the main noise is from the OAM mode of TC equal to 3.

Furthermore, we set the radius at 30 μm and vary the width from 6 μm to 12 μm. Fig. 5(a) shows the mode purity and the PER. It can be seen that the purity is close to 1 in the middle area and decreases at both sides, but the purity remains above 0.9 and the PER stays above 20 dB over almost all the bandwidth. When further increasing the width from 18 μm to 24 μm, the PER still keeps above 15 dB at low frequencies but becomes poor ($<$ 10 dB) at high frequencies. In this case, the purity is meaningless because only the purity in radial direction is considered and azimuthal direction ignored. In addition, the PER will decrease with increasing the slit width as well as with increasing the THz frequency at high frequencies. It is because that the

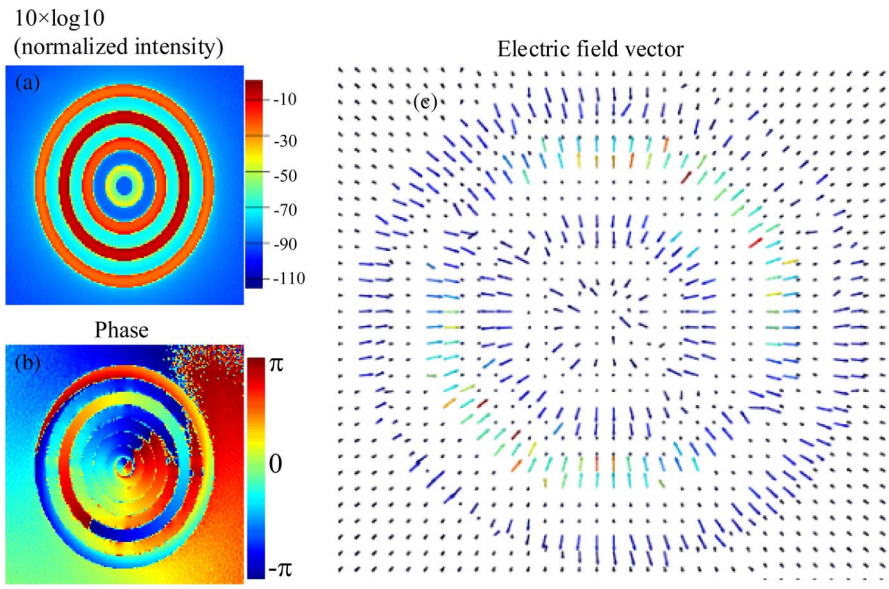

Fig. 6. Spatial distributions of (a) intensity, (b) phase, and (c) electric field vector of generated OAM beams at 1 THz.

transmittance of the azimuthal direction rapidly increases with the slit width divided by the wavelength, when the slit width is comparable to the signal wavelength. Fig. 5(b) displays the transmittance when the area of source is 200 μm $\times$ 200 μm. This case is similar to the one in Fig. 3(a).

When N slits are employed, they should have similar functions but keep a larger transmittance. As shown in Fig. 1(b), whose radiuses can be expressed as $R_n = R_1 + A(n-1)$ $(n = 1, 2 \ldots N)$, we set $R_1 = 5$ μm, $A = 14$ μm, and $N = 4$. Fig. 6 shows (a) output intensity distribution, (b) phase and (c) electric field vector at 1 THz. The intensity distribution is scaled by $10 \times \log_{10}$ (normalized intensity). One can see that a uniform intensity distribution in the azimuthal direction and a perfect helical phase distribution with TC equal to 1 is generated. The intensity of the third slit is much larger than the others; it is caused by the existence of transmission resonances at a radial direction which is similar to the transmission resonances of a rectangular slit for TM-polarized illumination [23]. This phenomenon is consistent with the aforementioned analyses where the deteriorated frequency does not appear at 1 THz when the radius of slit is not more than 55 μm. In addition, the purity is close to 1 at this frequency, as shown in Fig. 3(c). The output OAM beam is radially polarized which can be deduced from the electric field vector in Fig. 6(c). Thus, we can reasonably design the widths and the intervals of multiple concentric annuluses according to the analysis in Fig. 3 to avoid the deteriorated valley at the anticipant frequencies and keep larger transmittance.

4. Conclusion

We design a metal device containing circular subwavelength slits to convert the SAM of the incident THz beam to OAM. Our device has a similar function to the ASP. The PER is above 20 dB over the bandwidth ranging from 0.3 THz to 3 THz and the mode purity of TC $= 1$ (-1) is close to 1 over the middle area except the area near the deteriorated valley. We analyze the OAM spectrum and find the main noise comes from the OAM mode of TC $= -3$ (3). The deteriorated frequencies decrease with increasing the radius of slit. Our numerical results show that this device still keeps a high purity near both sides of the deteriorated valley. Thus, we can reasonably design the structure and parameters to avoid the deteriorated valley at the anticipant frequencies. When multiple slits are employed, they still has a high purity and keep a larger transmittance. The structure is simple with a size of micrometer order, which is an easy approach to broadband generation of the THz vortex beam.

References

[1] L. Allen, M. Beijersbergen, R. Spreeuw, and J. Woerdman, "Orbital angular momentum of light and the transformation of Laguerre-Gaussian laser modes," *Phys. Rev. A*, vol. 45, no. 11, pp. 8185–8189, Jun. 1992.

[2] Y.-S. Lee, *Principles of Terahertz Science and Technology: Proceedings of the International Conference, Held in Mainz, Germany, June 5–9, 1979*, vol. 170. Berlin, Germany: Springer, 2009.

[3] F. Lan, Z. Yang, L. Qi, X. Gao, and Z. Shi, "Terahertz dual-resonance bandpass filter using bilayer reformative complementary metamaterial structures," *Opt. Lett.*, vol. 39, no. 7, pp. 1709–1712, Apr. 1, 2014.

[4] Z. Huang, E. P. J. Parrott, H. Park, H. P. Chan, and E. Pickwell-MacPherson, "High extinction ratio and low transmission loss thin-film terahertz polarizer with a tunable bilayer metal wire-grid structure," *Opt. Lett.*, vol. 39, no. 4, pp. 793–796, Feb. 15, 2014.

[5] F. Yan, C. Yu, H. Park, E. P. Parrott, and E. Pickwell-MacPherson, "Advances in polarizer technology for terahertz frequency applications," *Int. J. Infrared Millim. Terahertz Waves*, vol. 34, no. 9, pp. 489–499, Sep. 2013.

[6] M. Navarro-Cía, P. Rodríguez-Ulibarri, V. Torres, and M. Beruete, "Terahertz quarter-wave plate based on subwavelength hole arrays," in *Proc. 7th EuCAP*, 2013, pp. 1256–1258.

[7] L. Meng *et al.*, "Optimized grating as an ultra-narrow band absorber or plasmonic sensor," *Opt. Lett.*, vol. 39, no. 5, pp. 1137–1140, Mar. 1, 2014.

[8] J. Grant, I. J. H. McCrindle, C. Li, and D. R. S. Cumming, "Multispectral metamaterial absorber," *Opt. Lett.*, vol. 39, no. 5, pp. 1227–1230, Mar. 1, 2014.

[9] J. He *et al.*, "Generation and evolution of the terahertz vortex beam," *Opt. Exp.*, vol. 21, no. 17, pp. 20230–20239, Aug. 26, 2013.

[10] L. Zhu *et al.*, "Experimental demonstration of basic functionalities for 0.1-THz Orbital Angular Momentum (OAM) communications," presented at the Opt. Fiber Commun. Conf., San Francisco, CA, USA, 2014, Paper M3K.7.

[11] M. Sakamoto, K. Oka, R. Morita, and N. Murakami, "Stable and flexible ring-shaped optical-lattice generation by use of axially symmetric polarization elements," *Opt. Lett.*, vol. 38, no. 18, pp. 3661–3664, Sep. 15, 2013.

[12] Y. Tokizane, K. Oka, and R. Morita, "Supercontinuum optical vortex pulse generation without spatial or topological-charge dispersion," *Opt. Exp.*, vol. 17, no. 17, pp. 14 517–14 525, Aug. 2009.

[13] Q. Zhan and J. R. Leger, "Interferometric measurement of the geometric phase in space-variant polarization manipulations," *Opt. Commun.*, vol. 213, no. 4–6, pp. 241–245, Dec. 1, 2002.

[14] M. Kang *et al.*, "Spatial splitting of spin states in subwavelength metallic microstructures via partial conversion of spin-to-orbital angular momentum," *Phys. Rev. A*, vol. 85, no. 3, pp. 035801-1–035801-5, Mar. 2012.

[15] M. Kang, J. Chen, X.-L. Wang, and H.-T. Wang, "Twisted vector field from an inhomogeneous and anisotropic metamaterial," *J. Opt. Soc. Amer. B, Opt. Phys.*, vol. 29, no. 4, pp. 572–576, Apr. 1, 2012.

[16] H. J. Lezec *et al.*, "Beaming light from a subwavelength aperture," *Science*, vol. 297, no. 5582, pp. 820–822, Aug. 2, 2002.

[17] J. Lin, P. Genevet, M. A. Kats, N. Antoniou, and F. Capasso, "Nanostructured holograms for broadband manipulation of vector beams," *Nano Lett.*, vol. 13, no. 9, pp. 4269–4274, Sep. 2013.

[18] Z. Zhou, Q. Tan, and G. Jin, "Cylindrically polarized vortex beams generated by subwavelength concentric Al metallic gratings," *J. Opt.*, vol. 13, no. 7, p. 075004, Jul. 2011.

[19] Y. Gorodetski, A. Niv, V. Kleiner, and E. Hasman, "Observation of the spin-based plasmonic effect in nanoscale structures," *Phys. Rev. Lett.*, vol. 101, no. 4, pp. 043903-1–043903-4, Jul. 2008.

[20] S. A. Schulz, T. Machula, E. Karimi, and R. W. Boyd, "Integrated multi vector vortex beam generator," *Opt. Exp.*, vol. 21, no. 13, pp. 16 130–16 141, Jul. 1, 2013.

[21] A. M. Beckley, T. G. Brown, and M. A. Alonso, "Full Poincare beams," *Opt. Exp.*, vol. 18, no. 10, pp. 10 777–10 785, May 10, 2010.

[22] A. M. Beckley, T. G. Brown, and M. A. Alonso, "Full Poincaré beams II: Partial polarization," *Opt. Exp.*, vol. 20, no. 9, pp. 9357–9362, Apr. 2012.

[23] F. Yang and J. R. Sambles, "Resonant transmission of microwaves through a narrow metallic slit," *Phys. Rev. Lett.*, vol. 89, no. 6, pp. 063901-1–063901-3, Jul. 2002.